# Computational Generation and Conformal Fabrication of Woven Fabric Structures by Harmonic Foliation

Yang Guo<sup>a,\*</sup>, Qian Ye<sup>b,\*</sup>, Xiaopeng Zheng<sup>c</sup>, Shikui Chen<sup>b</sup>, Na Lei<sup>c,\*\*</sup>, Yuanqi Zhang<sup>d</sup>, Xianfeng David Gu<sup>a</sup>

<sup>a</sup>Department of Computer Science, State University of New York at Stony Brook <sup>b</sup>Department of Mechanical Engineering, State University of New York at Stony Brook <sup>c</sup>DUT-RU International School of Information Science ℰ Engineering, Dalian University of Technology

<sup>d</sup>Division of Engineering and Applied Sciences, Harvard University

#### Abstract

This paper presents a framework for computational generation and conformal fabrication of woven thin-shell structures with arbitrary topology based on the foliation theory which decomposes a surface into a group of parallel leaves. By solving graph-valued harmonic maps on the input surface, we construct two sets of harmonic foliations perpendicular to each other. The warp and weft threads are created afterward and then manually woven to reconstruct the surface. The proposed computational method guarantees the smoothness of the foliation and the orthogonality between each pair of leaves from different foliations. Moreover, it minimizes the number of singularities to theoretical lower bound and produces the tensor product structure as glob-

<sup>\*</sup>Y.G. and Q.Y. contributed equally to this work.

<sup>\*\*</sup>Correspondence should be addressed to N.L.

Email addresses: yangguo@cs.stonybrook.edu (Yang Guo), qian.ye@stonybrook.edu (Qian Ye), zhengxp@dlut.edu.cn (Xiaopeng Zheng), shikui.chen@stonybrook.edu (Shikui Chen), nalei@dlut.edu.cn (Na Lei), kzhang@gse.harvard.edu (Yuanqi Zhang), gu@cs.stonybrook.edu (Xianfeng David Gu)

ally as possible. This method is ideal for the physical realization of woven surface structures on a variety of applications, including wearable electronics, sheet metal craft, architectural designs, and conformal woven composite parts in the automotive and aircraft industries. The performance of the proposed method is demonstrated through the computational generation and physical fabrication of several free-form thin-shell structures.

Key words: freeform surfaces, surface weaving, woven fabrics, thin-shell structure, foliation, harmonic map, conformal

#### 1. Introduction

The rapid development of additive manufacturing has enormously enhanced the possibility of manufacturing complex structures. However, the conventional planar-layered 3D printing techniques are still facing challenges, such as limited printable materials [1] and inconsistent printing quality [2]. Especially, when it comes to free-form shell structures, efforts for creating very fine tessellations and supporting structures are required to ensure a successful printing, which not only decelerate the process, but also introduce a tedious removal procedure [1]. Inspired by traditional woven fabrics, a method of constructing free-form shell structures by weaving is proposed to tackle the aforementioned barriers.

#### 1.1. Woven Fabric in Engineering

Generally speaking, woven fabrics are the textiles formed by interlacing two sets of threads (warp and weft) at right angles [3], as shown in Fig. 1. Possessing advantages, such as being lightweight, economy, and ease of implementation, woven structures have been widely used in the engineering,

from traditional apparel manufacturing to recently spreading fields, such as composites [4], metamaterial design [5, 6], and wearable electronics [7, 8].



Figure 1: Woven Fabric in Engineering: Left to right—A schematic diagram of regular planar woven fabric; The Airbus A350-900 constructed by more than 50% composite materials [9]; A scheme of self-charging E-textiles by Pu et al. [10]; A schematic diagram of 3D woven fabric by Drach et al. [11]

Woven composites have been proven an effective reinforcing material in aircraft and the automotive industry because of their performance as a combination of strength and toughness [4, 12, 13]. By further considering the fiber arrangement in the thickness direction, the 3D weaving technique has quickly been adopted [14, 15, 16, 17], especially in designing lattice metamaterial for damping and vibration control [5, 6, 18]. These multi-layer textiles can display notable characteristics such as enhanced stiffness along thickness direction [17], higher energy dissipation ability [19, 20], and stronger buckling mitigation capability [21].

E-textiles are woven fabrics comprising electronic elements. They can preserve the pros of conventional textiles as flexible and comfortable, as well as present functionalities, for instance, interacting with the environments or users [22, 23]. The e-textiles have been used as wearable electronics in tracking physical activity data [24], health monitoring [25], and energy harvesting [8].

In real industries, many applications demand woven fabrics on curved surfaces, e.g., woven protective clothing, composite automotive linings, smart wristbands made by e-textiles, and so on [26, 27, 28]. However, conventionally, the textiles are fabricated in plain and output as flat or roll-up sheets. As to conform to a curved surface, the fabrics will undergo large deformation [29, 30] or be cut and sewn. This fitting surface process breaks the continuity of the fibers, produces defects like wrinkles, local sliding, damages the mechanical properties, and even causes failures like splitting and delamination [31, 32, 33]. Thus, the trends in weaving directly to form a surface—conformal woven fabric— are emerging. [28, 23].







Figure 2: Architectures inspired by weaving: Left to right— The Weaving Pavilion by David Garcia Studio [34], the Woven Tower by Farris *et al.* [35], the God's eye pavilion by Georgiou *et al.* [36]

It is also worth noticing that at a large scale in engineering, e.g., architecture, the cutting edge designs are innovative and stylish. With the integration of mathematics, computer-aided design, and construction techniques, people can bring visual designs into reality. Landmarks with free-form geometries have broadened people's horizons, e.g., the *Sydney opera house*, the *Gherkin* in London, and the *Vessel* in New York. Given the observation that an artisan can achieve a complex 3D object (e.g., a basket with handles) by

straightforward approaches like braiding, weaving, and knotting, architects have been inspired to employ the logic of those textiles at the architectural scale [37, 38, 39]. Fig. 2 includes several woven architectural designs, which show the potential of weaving as an architectural technique. However, currently, the realization of these woven shell structures is operated case by case. A systematic way to extend the weaving technique to general surfaces is demanded [38, 39].

Thus, in this work, we propose a method-conformal fabrication- to address the issue of fabricating a surface by weaving. There are two main contributions to the work. First, the shape of the woven fabric is directly formed during weaving and conformal to the input surface. Moreover, the method is general in dealing with the surface with arbitrary topologies.

### 1.2. Conformal Fabrication by Weaving

Briefly, conformal fabrication of woven fabric is equivalent to forming an arbitrary curved surface by interlacing two groups of yarns at right angles. We can further recast the problem as a geometry question: covering the surface by orthogonal foliations. Mathematically, a foliation is a decomposition of the surface as a group of parallel leaves. Moreover, the conformal woven fabric should satisfy similar fabrication requirements as the conventional woven fabric: for each work-piece, the two sets of threads cross at right angles, and each of the threads is continuous. Fig. 3 shows an example of hand surface woven by two groups of paper strips.

Researchers have introduced several pioneering works regarding generating conformal woven fabric. Akleman *et al.* [40] presented a graph rotation system to convert a meshed surface to a thin-shell structure with plain-weave



Figure 3: Left to right: Computation of two orthogonal harmonic foliations (red loops and blue curves). The red (blue) foliations are converted to white (black) strips. The black and white strips are woven together to construct the human hand model.

appearance, also known as the one-up-one-down pattern. They further enriched the work to woven fabrics with the twill pattern [41] as well as applications on the digital fabrication of architecture designs [42]. However, The orthogonality of interlacing of threads, which is crucial for a woven object [43], is not guaranteed. The weaving strips are cyclic loops instead of two distinct sets as conventional weaving. Thus the physical fabrication process is neither intuitive nor easy. Besides, although adjustable by parameters, the weaving threads can not completely cover the surface and will leave gaps in the woven object. Those gaps will create stress or strain concentrations [44], and decrease the mechanical properties such as damage tolerance and fatigue toughness [45].

Apart from regular woven structures, the triaxial woven fabrics of which yarns braided at 60 degrees have gained people's attention. Vekhter *et al.* [46] proposed a vector field method to generate triaxial woven structures by solving an optimization problem. However, the robustness of the process needs improvement since the singularities of the problem depend on the initial

value. Similarly, Ayres *et al.* [47] presented a computational approach to approximate a meshed surface into triaxial woven structures with interlaced straight strips. Their method utilizes existing algorithms in the literature and thus is relatively easy for implementation.

Considering the fabrication requirement that weaving threads interlace at right angles (in other words, the woven unit cell is ideally to be rectangles), Takezawa et al. [48] proposed a method to fabricate a surface by paper strips created along the principal curvatures. The process is intuitive since there exist two orthogonal curvature lines through each non-umbilic point. However, at the umbilical points, the directions of the two principal curvatures coincide. Thus the induced weaving threads are non-regular, and therefore, the woven object fails to fulfill the fabrication requirements. The isolated segments will appear, and the woven unit cells are no longer rectangles or quadrilaterals, but highly irregular N-sided cells—arbitrary polygons.

Campen et al. [43, 49] introduced the dual strip weaving method that creates cyclic loops on a given surface and partitions it into quadrilateral patches. In particular, they computed the topological loops on a surface by minimizing an energy function that, for a single loop, penalizes the total length, the deviation from principle directions, and the geodesic curvature. Then they broadened the circles to stripes, cut them by vertical lines, and thus achieved the quadrilateral patches. However, the algorithm requires the surface can be divided into topological discs and strips generated by the method may have self-crossings with arbitrary angles.

Furthermore, in the literature of topology, surface foliation only admits even valence singularities. The results produced by Campen's process can

# be described as meromorphic quartic differentials, which we give a thorough treatment in [50].

The theory we use in this work to generate woven fabrics of a given surface is the so-called foliation theory. Mathematically, a foliation is a decomposition of the surface into a group of parallel leaves. Thurston [51] first introduced foliation theory to study diffeomorphisms on surfaces. The foliation has shown a deep connection with quadratic differentials on Riemann surfaces [51, 52]. In exceptional cases, when a quadratic differential has closed trajectories, the induced foliation tiles the surface by closed leaves [53]. In the field of computational geometry, Gu et al. [54] used the Hodge theory to compute holomorphic one-forms for the global conformal parameterization of a surface which is indeed a special case of holomorphic quadratic differential. Later, Lei et al. [55, 56, 57] introduced the foliation method to generate a regularized quadrilateral mesh. These works give us a theoretical base of computing foliations on a surface with arbitrary topology.

The rest of the paper is organized as follows: Section 2 briefly introduces the pipeline of the framework and summarizes the contributions of our method. Section 3 presents the detailed mathematics theory and algorithm regarding surface foliation, followed by the example of weaving the genus two surface and a hand surface model by craft-paper in Section 4. Section 5 evaluates the approximation accuracy of the woven structures to the input surfaces as well as the manufacturing requirements— the orthogonality of weaving angles. Section 6 summarizes the paper, discusses the pros and cons of the proposed method, and outlines the future work.

#### 2. Method Overview

The computational generation of woven fabric on arbitrary surfaces in this work utilizes the foliation theory. First, two families of orthogonal foliations are computed on a given surface (section 3.1, 3.2, 3.3). Then we decompose the surface into topological cylinders based on the foliation results (section 3.4). On each of the cylinders, we compute a quadrilateral mesh (section 3.5), in which the quads refer to woven unit cells. To conformally fabricate the woven structure, we first generate weaving strips from the quad-mesh (section 4.1). Next, we unfold the strips onto the 2D-plane, cut them out on physical materials, e.g., construction paper, and then get two orthogonal groups of weaving threads (section 4.2). By interlacing the warp and weft threads in a particular order (such as plain weaving or twill), we can obtain a woven structure that is conformal to the input surface (section 4). The contributions of the presented framework can be summarized as follows:

- This paper proposes a systematic solution to physically realizing the conformal woven fabrics. The methodology is general in geometries and scales: one can form a surface with arbitrary topology by interlacing two sets of threads generated by our algorithm; the size of the threads are adaptable in considering the accuracy and dimension of the applications, such as micro or mesoscale in wearable electronics, sheet metal craft, conformal woven composites, and a larger scale in architectural designs.
- From the mathematical point of view, the weaving structure generated by our method has the least number of singularities and no dangling

leaves, which increases the mechanical strength and reduces the complexity of assembly.

- From the fabrication aspect, the free-form surface can be directly shaped during the weaving process: the conventional indirect procedures of prefabricating the woven fabrics and then finalizing the shape are omitted.
- From the designer perspective, the proposed harmonic foliations method guarantees smoothness, orthogonality, and global tensor product structure, which preserves the aesthetic value as well as enhances the mechanical properties of the woven fabrics.

# 2.1. Theory of Topological Foliation

In this section, we briefly introduce the classic foliation theory as the background information. According to the definition of topological foliation, a foliation can tile a surface by infinitely many parallel curved leaves. Specifically, a leaf is a curve on the surface, which is either a closed-loop or a infinite spiral. There exist infinitely many topological foliations on a high genus surface. Roughly speaking, any measured foliation on a Riemann surface is equivalent to the horizontal trajectory of a unique holomorphic quadratic differential, and all the quadratic differentials form a finite dimensional linear space [52]. Fig. 4 shows a topological foliation on a genus g = 5 surface. In the neighborhood of a normal point, all the leaves are parallel to each other. In general cases, in the neighborhood of a singularity, three strands of leaves meet together. There are 4g-4 singularities. The leaves through singularities are called critical leaves. A foliation with all the leaves closed loops is called a finite measured foliation. The critical leaves of a finite measured foliation

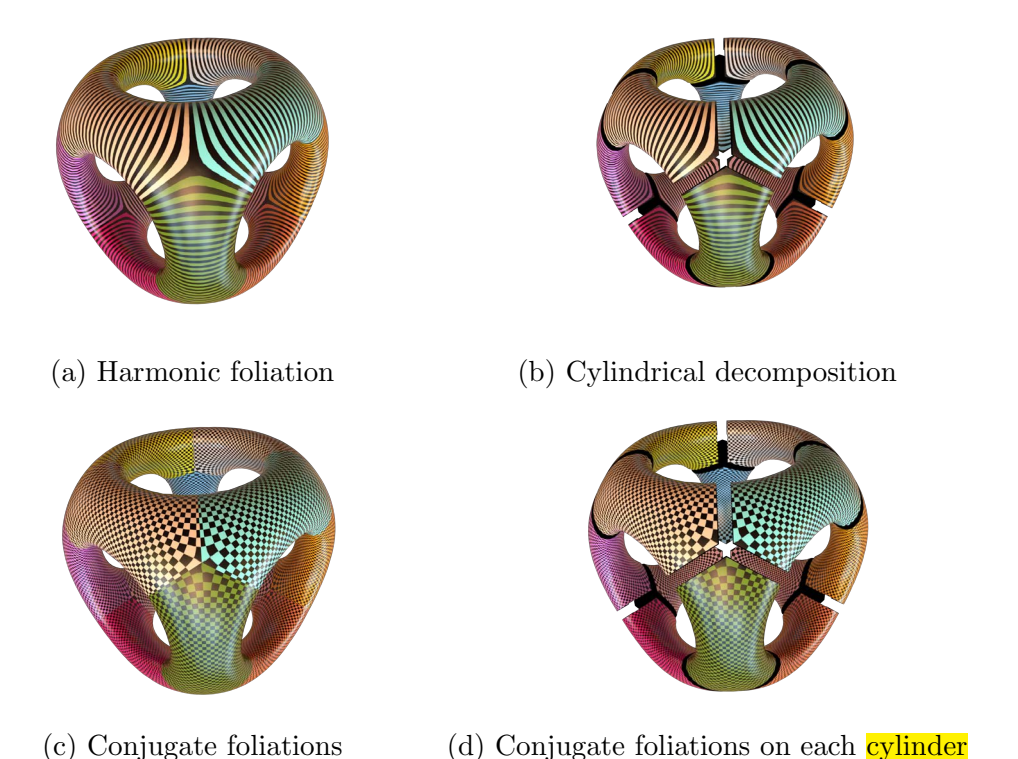


Figure 4: The global structure of a foliation on a genus 5 surface. In (a), leaves of the foliation are shown in black and colored strips. In (b), the high genus surface can be decomposed into cylinders by cutting through critical leaves. Subfigure (c) shows the conjugate foliation together with the original one, and (d) shows the original and conjugate foliations on the induced cylindrical decomposition.

form a finte graph, which divides the surface into 3g-3 topological cylinders, rendered using different colors in Fig. 4. On each cylinder, one can find another topological foliation orthogonal to the current one. By collecting their leaves, we obtain a global topological foliation orthogonal to the original one—conjugate foliations. While in special cases, the singularities may merge together, such as those of holomorphic one-forms. For a holomorphic one-form, there are 4 critical leaves through each singularity, and there are totally

2g-2 singularities. The square of a holomorphic 1-form is a holomorphic quadratic differential.

## 3. Computational Generation of Foliations

#### 3.1. Harmonic Foliation

By mapping each leaf in a finite measured foliation to a point, we get the *Ribbon graph* of the foliation (see Figure 5 (a)). Each arc of the Ribbon graph corresponds to a cylinder, and each node represents a critical leaf. The foliation can be reconstructed from its Ribbon graph as follows: we compute a harmonic map from the surface to the graph, then the preimage of each point of the graph gives a leaf. Because the foliation is induced by a harmonic map, we call it a *harmonic foliation*. The harmonic foliation is very smooth, therefore with high aesthetic value. Furthermore, a unique harmonic foliation can be found that is orthogonal to the original one (the details will be discussed in section 3.4). We employ this pair of orthogonal harmonic foliations for fabrication purposes. In the following discussion, all the foliations refer to harmonic foliations, unless otherwise stated.

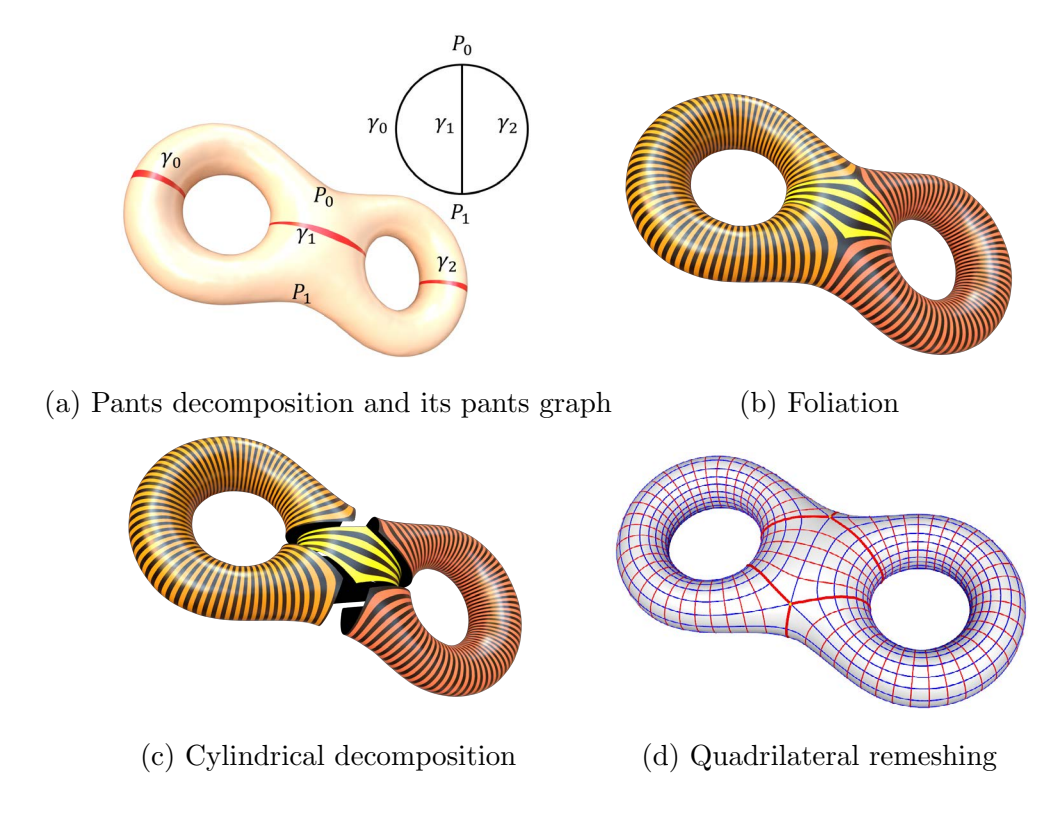


Figure 5: Foliation generation pipeline.

A finite measured surface foliation decomposes the surface into a family of closed loops, such that the decomposition has local tensor product structure. First, we explain the algorithm for a high genus closed surface. The progress is visualized in Fig. 5 and Algorithm. 1. Then we extend the method to general topologies in section. 3.6.

# 3.2. Pants Decomposition

As shown in Fig. 5 frame (a), the first step is pants decomposition [58], which is carried out automatically using the algorithm described in [59]. Given a genus g > 1 closed surface S, it divides the ambient space into two

connected components, the finite one is the interior volume; the infinite one is the exterior volume. A loop on the surface is called a handle loop, if it is homotopic to a point in the interior volume, but not homotopic to a point in the exterior volume; a loop is called a tunnel loop, if it is homotopic to point in the exterior volume, and not homotopic to a point in the interior volume. According to Dey's work  $\begin{bmatrix} 60 \end{bmatrix}$ , there are uniquely g handle loops and g tunnel loops that form a homotopy group basis of the surface. We use their algorithm to find g handle loops. Then we slice the surface along these handle loops to obtain a topological sphere with 2g boundaries.

Given a topological sphere with n boundaries, each time we choose a pair of adjacent boundary loops, say a and b, then compute a loop c enclose them, namely c is the product of a and b in the homotopy group. We slice the surface along c to divide the surface into connected components, one component is a topological sphere with three boundary loops a, b, and c, namely a pair of pants, the other is a topological sphere with n-1 boundaries. We repeat this procedure inductively, each time to cut off a pair of pants, and eventually decompose the surface into 2g-2 pairs of pants,  $\{P_1, P_2, \dots, P_{2g-2}\}$ , by  $3g-3=3\times(2g-2)/2$  cutting curves  $\{\gamma_1, \gamma_2, \dots, \gamma_{3g-3}\}$ .

A pants decomposition can be represented as a graph G, the so-called pants decomposition graph, where each pair of pants  $P_i$  is represented as a node  $n_i$ , and each cutting loop  $\gamma_j$  is denoted by an edge  $e_j$ . Suppose on the surface S, the cutting loop  $\gamma_i$  is shared by two pairs of pants  $P_j$ ,  $P_k$ , then in the graph G, the arc of  $e_i$  connects nodes of  $n_j$  and  $n_k$ . Furthermore, we associate a positive weight  $h_i > 0$  for each edge  $e_i$  in the pants decomposition graph. We use  $(G, \mathbf{h})$  to denote the pants decomposition graph G with the

weights  $\mathbf{h} = (h_1, h_2, \dots, h_{3g-3})$ , and call it the weighted pants decomposition graph. The weights can be used to adjust the strip widths.

According to [61], two foliations are equivalent if they differ by a surface diffeomorphism homotopic to the identity. Each equivalence class of foliations is equivalent to the horizontal trajectories of a unique holomorphic quadratic differential. All the holomorphic quadratic differentials form a linear space of 6g - 6 dimension, where g is the genus of the surface. The combinatorial structure of the graph, and the weights determines uniquely the holomorphic quadratic differential, therefore the class of the foliations. We refer readers to [61] for thorough theoretical treatment.

# 3.3. Generalized Harmonic Map

As shown in Fig. 5 frame (b), the second step is to compute a foliation based on a harmonic map between the surface and the weighted pants decomposition graph  $(G, \mathbf{h})$ .

The weighted pants decomposition graph  $(G, \mathbf{h})$  can be treated as a *metric* space, where the distance between two points  $p, q \in G$  is defined as the length of the shortest path connecting them, and denoted as  $d_{\mathbf{h}}(p, q)$ .

Given a mapping  $f:(S,\mathbf{g})\to (G,\mathbf{h})$ , the pre-image of a node is called a *critical leaf*, and the union of critical leaves is called the *critical graph*, denoted as  $\Gamma\subset S$ . In general, the critical graph is of 0 measure, then we can define the *harmonic energy* of the mapping f,

$$E(f) := \int_{S \setminus \Gamma} |\nabla_{\mathbf{g}} f|^2 dA_{\mathbf{g}}. \tag{1}$$

If f minimizes the harmonic energy, then f is called a harmonic map. Wolf [62] proved the existence and the uniqueness of the harmonic map. The

preimage of each non-node point is a closed loop on the original surface. All such closed loops compose a foliation  $\mathcal{F}$ . The Ribbon graph of the foliation  $\mathcal{F}$  is exactly  $(G, \mathbf{h})$ .

In practice, the surface is approximated by a triangular mesh M = (V, E, F). We use  $[v_i, v_j]$  to represent an edge connecting the vertices  $v_i$  and  $v_j$ . The harmonic energy of a map  $f: M \to (G, \mathbf{h})$  is given by

$$E(f) := \frac{1}{2} \sum_{[v_i, v_j]} w_{ij} d_{\mathbf{h}}(f(v_i), f(v_j))^2,$$

where  $d_{\mathbf{h}}(\cdot, \cdot)$  is the shortest distance between two points on the graph,  $w_{ij}$  is the *cotangent edge weight*. Suppose two faces  $[v_i, v_j, v_k]$  and  $[v_j, v_i, v_l]$  share the edge  $[v_i, v_j]$ , then

$$w_{ij} = \cot \theta_k^{ij} + \cot \theta_l^{ji},$$

where  $\theta_k^{ij}$  represents the corner angle at the vertex  $v_k$  in the face  $[v_i, v_j, v_k]$ . We use the non-linear heat flow method to compute the harmonic map.

- 1. We homotopically deform  $\gamma_i$  to sweep a cylinder  $C_i$ , such that the union of all the cylinders cover the whole surface.
- 2. Each cylinder  $C_i$  is mapped to the edge  $e_i$ , this constructs the initial map f.
- 3. We diffuse the map to reduce the harmonic energy, until it converges to the harmonic map.

The diffusion process is as follows: at each step, we move the image of each vertex to the weighted geodesic center of the images of its neighbors. Suppose after the k-th iteration, we have obtained the mapping  $f_k: M \to G$  already, vertices  $\{v_j\}$ 's are adjacent to the vertex  $v_i$ , the weighted geodesic center of

 $\{f_k(v_j)\}$ 's is defined as

$$c_k(v_i) = \operatorname{argmin}_{q \in G} \sum_{j=1}^n w_{ij} d_{\mathbf{h}}(f_k(v_j), q)^2.$$

The diffusion process moves the image of  $v_i$  to the weighted geodesic center,  $f_{k+1}(v_i) \leftarrow c_k(v_i)$ . By repeating this procedure, the mapping sequence  $\{f_n\}$  converges to the harmonic map.

The harmonic foliation is composed of the leaves, each leaf is a preimage of a point in the graph,  $\mathcal{F} = \{f^{-1}(p)|p \in G\}.$ 

According to Schoen's generalized harmonic mapping theory [63], if the target space is a non-positive-curved metric space, then each homotopy class of the mapping has a unique harmonic map. In our case, the target is the weighted pants decomposition graph, which is a non-positive-curved metric space. If the homotopy class of mapping from the surface to the graph is trivial, namely all loops on the surface are mapped to the loops on graph that can shrink to a point, then the final harmonic map is trivial (the image is the single point). In order to prevent this, we specify the homotopy class by the initial map, as shown in Figure the loops circling the tunnels are mapped to the non-trivial loops on the graph. This guarantees the final map is non-trivial.

# 3.4. Cylindrical Decomposition

As shown in Fig. 5 frame (c), the preimages of the nodes form the critical graph  $\Gamma$ , the surface is sliced along  $\Gamma$  and decomposed into 3g-3 topological cylinders. Different cylinders are rendered using different colors, all the leaves within one cylinder are homotopic to each other.

# Algorithm 1: Surface Foliation Algorithm for Close Surface.

```
Input: A closed surface S with genus g > 1 and a threshold ε
Output: A foliation F of S
1 Construct a pants decomposition of S;
2 Construct the pants decomposition graph G, assign the edge weight h to G;
```

- **3** Construct an initial map  $f: \mathcal{S} \to G$  by mapping each pair of pants to the corresponding node;
- 4 Compute the initial harmonic energy E;

```
5 while true do
          E_0 \leftarrow E;
          foreach vertex v_i \in \mathcal{S} do
               f(v_i) \leftarrow \operatorname{argmin}_{q \in G} \sum_{j=1}^{n} \omega_{ij} d_{\mathbf{h}}(f(v_j), q)^2;
          end
 9
          Calculate the harmonic energy E;
10
          if |E - E_0| < \varepsilon then
11
               break;
12
          \quad \text{end} \quad
13
14 end
15 foreach p \in G do
          Compute the leaf f^{-1}(p) \in \mathcal{S};
17 end
18 Return the foliation \mathcal{F} consisting of all leaves;
```

For each edge  $e_i \in G$ , its preimage is a cylinder  $C_i$ . The restriction of the harmonic map on the cylinder  $C_i$ ,  $f_i := f|_{C_i}$ , can be treated as a harmonic function,  $f_i : C_i \to [0, h_i]$ . The gradient of  $f_i$  can be expressed explicitly. Suppose a face  $[v_p, v_q, v_r]$  is in the cylinder  $C_i$ , the gradient of the piece-wise linear map  $f_i$  on this face is

$$\nabla f_i := \mathbf{n} \times (f_i(v_r)(v_q - v_p) + f_i(v_p)(v_r - v_q) + f_i(v_q)(v_p - v_r))$$

where **n** is the normal to the face, by abusing the symbols,  $v_r$  represents the position of the vertex  $v_r$ . The *Hodge star* operator is defined as

$$^{\star}\nabla f_i := \mathbf{n} \times \nabla f_i.$$

When the mesh triangulation is refined enough, the integration lines of the vector field  ${}^*\nabla f_i$  give the so-called *conjugate foliation*  $\mathcal{F}^*$  that is orthogonal to the original foliation  $\mathcal{F}$ . According to [61] the conjugate foliation  $\mathcal{F}^*$  itself is harmonic as well. The conjugate foliation is depicted in Fig. 5 frame (d), whose leaves are the blue loops.

#### 3.5. Quadrilateral Remeshing

Fig. 5 frame (d) illustrates the quadrilateral remeshing step. Basically, given a pair of conjugate foliations  $\{\mathcal{F}, \mathcal{F}^*\}$ , we can select some leaves to form a quadrilateral tessellation of the surface.

In more details, each cylinder  $C_i$  has two boundaries,  $\partial C_i = \tau^+ - \tau^-$ . We can find the shortest path  $\gamma$  connecting  $\tau^+$  and  $\tau^-$ . We slice  $C_i$  along  $\gamma$  to get a topological quadrilateral,  $D_i$ . The integration of a pair of vector fields  $({}^*\nabla f_i, \nabla f_i)$  gives a parameterization  $\varphi_i : D_i \to \mathbb{R}^2$ , picking a base point

$$p_0 \in D_i$$
,

$$\varphi_i(p) = \int_{p_0}^p ({}^*\nabla f_i, \nabla f_i) dr,$$

where the integration path r(t) from  $p_0$  to p is arbitrarily chosen within  $D_i$ . It was proven in [64] that the parameterization  $\varphi_i$  is angle-preserving, and maps the planar regular grids to the surface. The planar horizontal and vertical lines are mapped to red and blue loops on the surface respectively. As shown in Fig. 5, because the parameterization is a diffeomorphism and angle-preserving, the red/blue leaves are orthogonal, and the quadrialteral cells are similar to squares. Moreover, the user can specify density of the planar regular grid in order to determine the resolution of the quadrilateral mesh on surface; since each of the quadrilaterals represents a woven unit cell, the accuracy and scale of the woven surface can be adjusted accordingly.

#### 3.6. General Cases

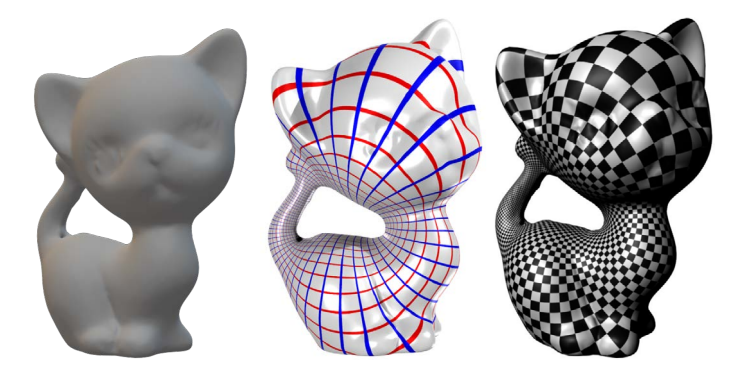


Figure 6: Conjugate foliations on a genus one surface.

# 3.6.1. Genus One Closed Surface

Fig. 6 shows a pair of conjugate foliations on a genus one closed surface. First, we compute the handle loop  $\gamma$ , set the weight to be the unit, then find a harmonic map from the surface to  $\gamma$  with the unit weight,  $f: S \to \gamma$ . The harmonic map induces a foliation  $\mathcal{F}$ , whose leaves are the red loops. Locally, f can be treated as a harmonic function. Similarly, we use the Hodge star operator to get the vector field  ${}^*\nabla f$ , and the integration of  ${}^*\nabla$  gives the conjugate harmonic foliation  $\mathcal{F}^*$ , whose leaves are the blue loops in Figure 6.



Figure 7: Foliation on an annulus.

If a topological annulus (Euler characteristic of 0) is given, we use the double cover technique to convert it to a topological torus as follows: we get a copy of the annulus, reverse the orientation, then glue the annulus with the reversed copy along the corresponding boundaries, to obtain a symmetric closed topological torus. Then we compute a symmetric holomorphic one-form on the torus, see Figure

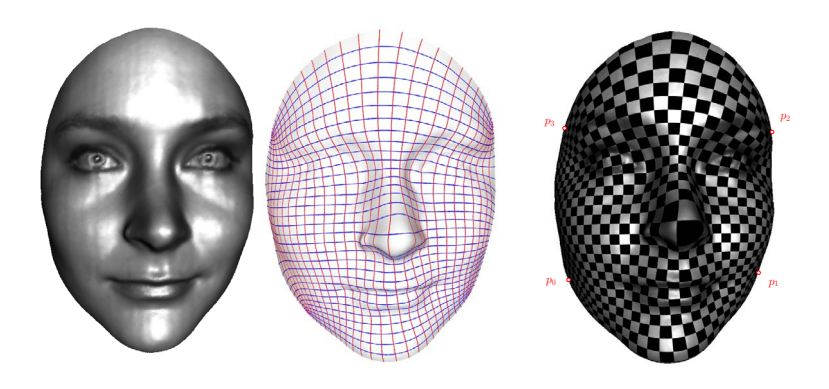


Figure 8: Conjugate foliations on a facial surface.

# 3.6.2. Topological Disk

As shown in Figure 8, given a genus zero surface M with a single boundary (a topological disk), we can select four boundary points  $\{p_0, p_1, p_2, p_3\}$ , which divide the boundary of the surface into four segments,  $\{\gamma_0, \gamma_1, \gamma_2, \gamma_3\}$ , such that  $\partial \gamma_i = p_{i+1} - p_i$ .

Then we perform the *double covering* operator: make a copy of M, denoted as  $\bar{M}$ , reverse the orientation of all faces of  $\bar{M}$ , then glue M and  $\bar{M}$  along the boundary segments  $\gamma_0$  and  $\gamma_2$ , to form a topological cylinder  $\tilde{M}$ .

Next, we compute a harmonic map from the doubled mesh  $\tilde{M}$  to the unit interval,  $f: \tilde{M} \to [0,1]$ , such that the boundary loops of  $\tilde{M}$  are mapped to the end points of the interval. Then level sets of f gives a foliation  $\mathcal{F}$ . The integration curves of  ${}^*\nabla f$  gives the conjugate foliation  ${}^*\mathcal{F}$ . The restriction of the  $\{\mathcal{F}, {}^*\mathcal{F}\}$  on the original mesh gives the desired pair of conjugate foliations.



Figure 9: Foliation on a topological sphere.

Given a topological sphere (Euler characteristic of 2), we can conformally map it onto the canonical unit sphere, and use the stereo-graphic projection to map it on the complex plane. Then we can pull back foliations on the plane to the sphere, see Figure

# 3.6.3. Open Surfaces with Negative Euler Numbers

Given a surface M,  $\chi(M) < 0$ , with boundary curves  $\partial M = \{\gamma_1, \gamma_2, \cdots, \gamma_n\}$ , we first use double covering to obtain a symmetric closed surface  $\tilde{M}$ . Then we extend  $\{\gamma_1, \gamma_2, \cdots, \gamma_n\}$  to a set of cutting loops, generate the pants decomposition, and compute the harmonic map from  $\tilde{M}$  to the pants decomposition graph, in turn obtaining a foliation  $\mathcal{F}$ . By construction, the boundary loops of the original mesh  $\{\gamma_i\}$  become the leaves of  $\mathcal{F}$ . Furthermore, we use the Hodge star operator to obtain the conjugate foliation  ${}^*\mathcal{F}$ . The restriction of the  $\{\mathcal{F}, {}^*\mathcal{F}\}$  on the original mesh gives the desired pair of conjugate foliations.

Fig. 10 demonstrates the foliation  $\mathcal{F}$  on a genus zero surface with multiple boundaries. The cat model is punctured through the bottom of the feet, the tip of the tail and the eyes, therefore there are 7 boundary components. The



Figure 10: Foliations on a genus 0 surface with multiple boundaries. hand model in Fig. 3 is also of genus zero with 6 boundaries, including 5 punctures at the finger tips.

# 4. Conformal Fabrication of Woven Fabric on Surfaces

# 4.1. Strip Generation and Unfolding

As stated in Chapter 3, the foliation generation pipeline produces a pair of conjugate foliations  $\{\mathcal{F}, \mathcal{F}^*\}$ , and a quadrilateral mesh (quad mesh), still denoted as M. The mesh M is approximated by a polyhedral surface. Each cell  $\sigma_i$  on M has four boundary edges with alternated colors, for instance,  $\{red, blue, red, blue\}$ . Starting from a cell  $(\sigma_i)$  adjacent to a critical leaf, we sequentially connect adjacent cells

$$s = \{\sigma_0, \sigma_1, \sigma_2, \cdots, \sigma_n\}$$

where  $\sigma_i$  and  $\sigma_{i+1}$  share a red (blue) edge for  $0 \le i \le n$ , and call s a horizontal strip (vertical strip). The quad-mesh M is decomposed into a family of horizontal strips, and a family of vertical strips. Each cell belongs uniquely to one horizontal strip and one vertical strip. The union of all strips covers

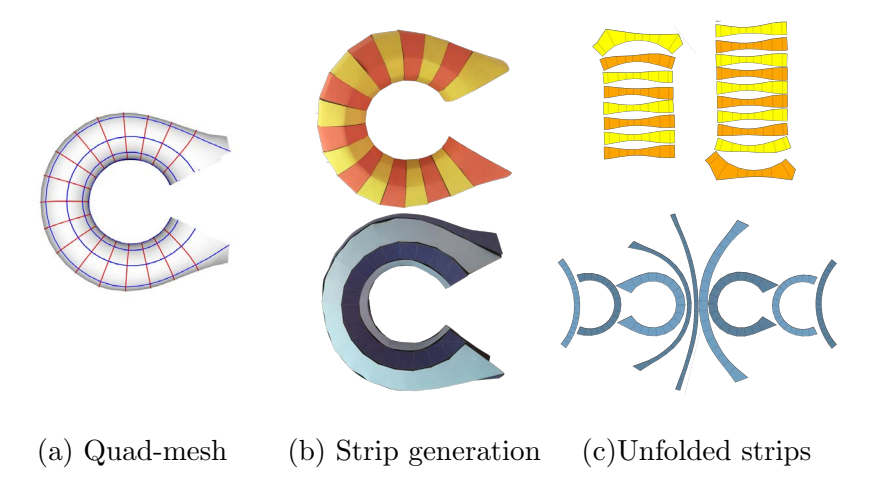


Figure 11: Strip generation on a C shape surface

the whole mesh twice. As shown in Fig. 11, we apply the strip generation on the C shape surface. According to the computed quad mesh as Fig. 11 frame (a), we can generate the horizontal strips and vertical strips as shown in Fig. 11 frame (b) the top and bottom, respectively.

The input surface is represented as a triangular mesh, and it is converted to a quadrilateral mesh using the obtained foliation. First, the vertex positions are sampled on the triangle mesh where one horizontal trajectory intersects a vertical trajectory; then the vertices are connected by edges by tracing the horizontal and vertical trajectories; then the vertices are optimized to ensure each quadrilateral face is planar using the method introduced in [65]. The edges are divided to horizontal and vertical edges. Quad faces are connected by horizontal edges to form vertical strips, and by vertical edges to form horizontal strips. we computationally cut them along vertical edges or horizontal edges. All the strips can be isometrically embedded onto the plane. The horizontal and vertical strips are overlapped, and the two layers together

cover the whole surface. This procedure is called unfolding. As Fig. 11 frame (c), the top and bottom figures are the unfolded horizontal and vertical strips of the C shape surface, respectively.

# 4.2. Weaving Process

After generating and unfolding the strips numerically, we can pack them together to fill a planar material. In this work, we use the construction paper as an example. By cutting along the contours of the strips manually by scissors, or automatically by a laser cutter, we can physically get the two groups of pieces for weaving. In the practical weaving, the horizontal and vertical strips work like weft and warp threads, respectively.

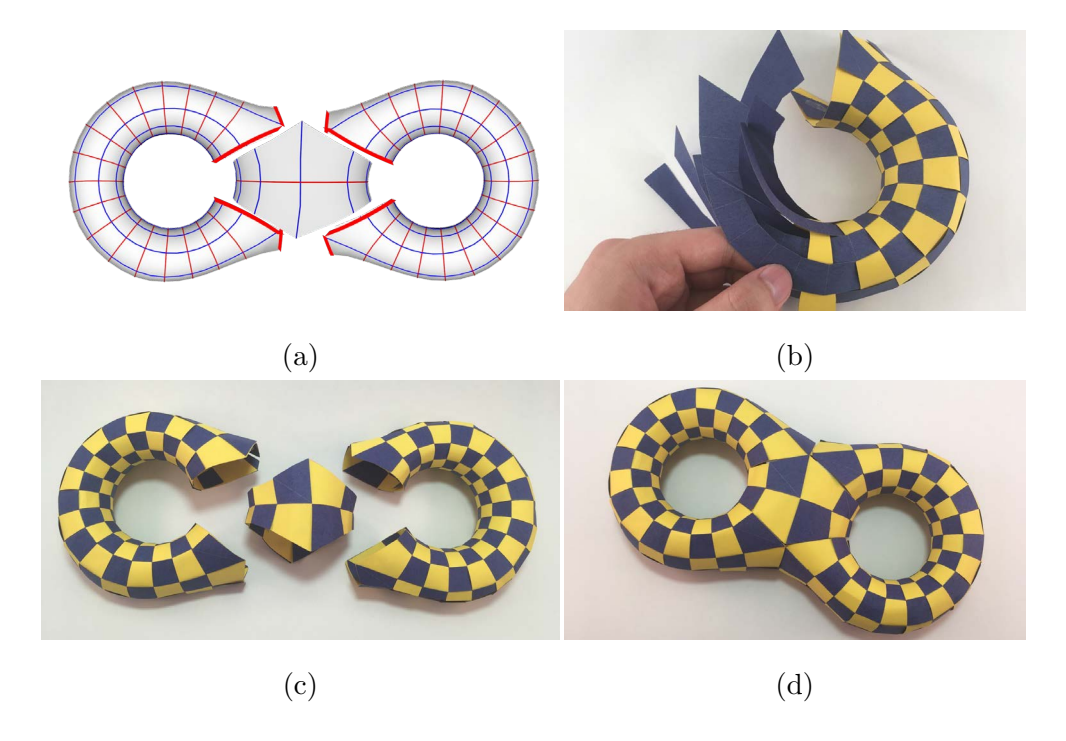


Figure 12: The Conformal Fabrication of Genus Two Model.

We demonstrate the conformal fabricating of a genus two surface as an

illustrative example. As stated in Section 3, the surface can be decomposed into three topological cylinders following their critical leaves (Fig. 12(a)). We can weave each of the parts individually (Fig. 12(b) and Fig. 12(c)), and assemble them together when finishing to reconstruct the surface (Fig. 12(d)). Similar to the fabrication of woven composite where a matrix material (e.g. epoxy resin) is used to bond the fibers [66], we glue each pair of the unit cells to add rigidity to the structure. The horizontal (vertical) strips are made of bright yellow (navy blue) paper.



Figure 13: Strips for the genus two surface model. The bottom row shows the horizontal (white) strips, the top row shows the vertical (black) strips.

Notably, the scales of the strips can be accommodated to the dimensional and accuracy requirements. As shown in Fig. 13, the genus two surface with higher accuracy are fabricated with denser threads. Fig. 14 shows the different stages of the assembly, each cylinder is constructed individually,



Figure 14: Fabrication by plain weaving.

then all the cylinders are glued together. In order to obtain a black/white alternate pattern over the surface, it suffices to ensure the number of wefts and warps are even during the foliation computation procedure, and ensure adjacent threads from different topological cylinders have different color during the weaving process.

# 4.3. Weaving High Curvature Variation Surfaces

As to show the generality of the proposed method, we apply the technique to fabricate a human hand surface, which consists of high curvature variations. As shown in Fig. 15, the hand surface is divided into five parts by the critical leaves; according to the computed quad mesh, the weaving strips are generated in each section; finally, the five regions are woven and glued together.

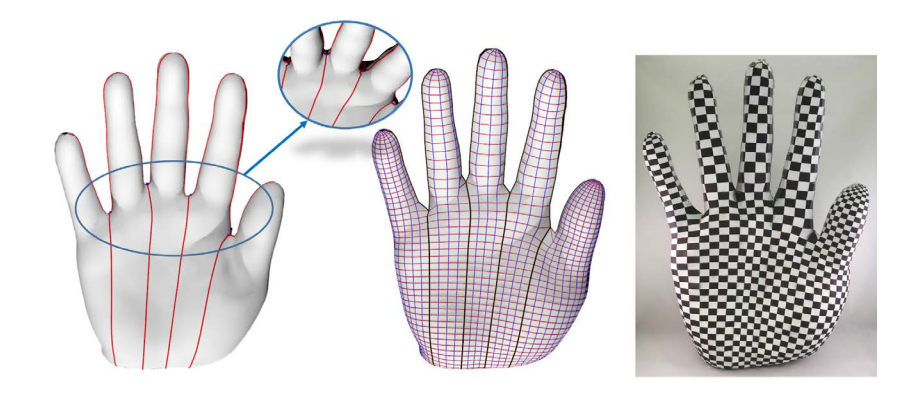


Figure 15: Conformal fabrication of woven fabric on hand surface

# 4.4. Weaving with Different Styles

Adopting the idea from conventional weaving, a variety of weave architectures can be achieved by interlacing the warp and weft threads in different orders. The most common weaving pattern is the aforesaid plain weave; each warp thread passes up-and-down each weft thread. Visually, objects constructed by plain weave have a checkerboard-like appearance. Fig. 16(a) shows the constructed model by plain weave. The plain weave creates the maximum amount of interlacing area, thus offers the most reinforcement on the surface.



Figure 16: Conformal fabrication of the genus two model with different weave styles

By adhering all horizontal threads under vertical threads at each paired unit cell, or vice versa, we get a two-layer object, as shown in the Fig. 16(b) and Fig. 16(c). Both threads can cover the surface without gaps. Moreover, the twill woven fabric shows a diagonal parallel style. A typical two by two twill patter is done by interlacing the warp thread over two weft threads and then under two weft threads, as shown in Fig. 16(d). The twill serves more flexible than plain weave since the less interlacing areas. All of these construction methods will precisely recover the weaving structure, which shows the compatibility of the proposed method in different weaving textures. Dur-

ing the construction process, no stretching will happen and the bending only appears at edges and possibly diagonal on each unit cells. The surface will be automatically shaped while weaving instead of manually adjusted.

# 5. Accuracy Evaluation

In this section, we evaluate the accuracy of our method on 6 prototypes: a hand model (Fig. 3), one higher precision (Eight model in Fig. 13 and Fig. 14) and 4 lower precision genus two surfaces (Fig. 16). The computational pipeline is automatic, the weaving strips are produced by a laser engraving and cutting machine, and the assembly process is straightforward. Curvature is automatically formed as neighboring paired cells adhere. The whole process does not need the user to have any professional knowledge. Table 1 summarizes the physical data of constructed paper models.

Models	Length (cm)	Width (cm)	Height (cm)	Weight (g)
Eight (L)	65.3	31.6	9.17	99.2
Eight (S)	25.4	12.5	4.24	17.0
Hand	39.8	11.0	55.7	70.9

Table 1: Size and weight of constructed paper models.

#### 5.1. Angle Deviation

As stated in Section. 1, the interlacing angles of each weft and warp are ideally to be 90 degrees. In our method, the pair of conjugate harmonic foliations  $(\mathcal{F}, \mathcal{F}^*)$  induce global conformal (angle-preserving) parameterizations onto 2D domains; therefore, theoretically the horizontal (red) and vertical

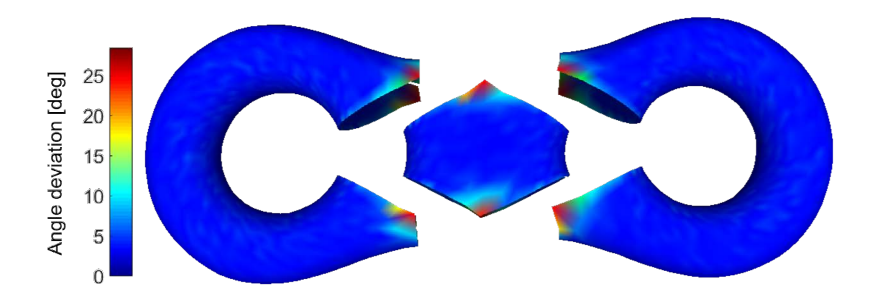


Figure 17: Angle deviation. This measures deviation of intersection angles from 90 degree. (blue) leaves are orthogonal apart from the singularities. The orthogonality cannot be guaranteed near the singularities. As to evaluate the variation of intersection angles from 90 degrees, the angle deviation at each vertex is computed using the equation below:

Angle Deviation(v) = 
$$\frac{1}{k} \sum_{i=1}^{k} |\alpha_i - 90^{\circ}|$$

where  $\alpha_i$  is an adjacent inner angle at vertex v, and k is the total number of  $\alpha_i$  at the vertex. Figure 17 shows the contour plot of the angle deviations on the genus two surface, the cross angles show a variability of 10 to 25 degrees at the singularity areas. The angle deviations data for all the woven models are reported in Table 2. Among all the models, the maximum angle deviation is 54 degrees (i.e., the angle itself is 36 degrees), and the average deviation is less than 10 degrees.

## 5.2. Surface Distance and Area Distortion Error

To evaluate how close the reconstructed surface is to the input surface, we assess the surface distance error between them explicitly using the Hausdorff distance [67]. For each woven unit—the unit cell on the generated quad

		Angle deviation		Surface distance		E <sub>Area</sub> Avg [%]
Models	# of quads (row,col)	E <sub>Ang</sub> Max [deg]	E <sub>Ang</sub> Avg [deg]	E <sub>Dis</sub> Max [%]	E <sub>Dis</sub> Avg [%]	LArea AVE [70]
Face	(15,16)	34.2	3.08	6.52	0.578	6.49
Face	(45,48)	34.5	0.93	1.43	0.0769	2.71
Face(K)	(45,48)	50	1.31	1.52	0.124	2.76
Face(K-area)	(45,48)	47.5	0.905	0.503	0.09	1.93
Thumb	(50,18)	37.9	2.32	1.56	0.127	0.198
Index finger (front)	(50,4)	47.5	1.75	1.6	0.162	0.774
Index finger (rear)	(50,6)	23.1	1.36	0.736	0.15	0.748
Mid finger (front)	(50,4)	39.8	1.4	0.79	0.13	0.574
Mid finger (rear)	(50,6)	32.5	1.18	0.833	0.128	0.878
Ring finger (front)	(50,4)	39.6	1.5	0.938	0.178	0.709
Ring finger (rear)	(50,4)	23.5	1.68	0.719	0.174	0.628
Baby finger	(50,16)	32.7	1.73	1.44	0.142	0.561
Eight(left)	(9,18)	40.7	2.45	2.1	0.567	5.34
Eight(right)	(9,18)	39.5	2.27	3.14	0.566	4.99
Eight(mid)	(13,2)	29.6	7.05	1.91	0.682	2.79
Eight(left)	(65,35)	43.5	0.59	0.349	0.0507	2.14
Eight(right)	(65,35)	43.5	0.548	0.208	0.0499	1.65
Eight(mid)	(10,59)	54	0.814	1.19	0.0452	3.73

Table 2: Summary of computational errors and time.  $E_{Ang}Max$  and  $E_{Ang}Avg$  are maximal and average angle error, which measures the deviation of the intersection angle from a right angle.  $E_{dist}Max$  and  $E_{dist}Avg$  are statistics of maximal and average distance errors, which are measured at each quad as the distance between the input surface and the reconstructed surface, and then normalized by the length of the foliation corresponding to that quad.  $E_{Area}Avg$  measures the average area distortion.

mesh, we measure the maximum distance between quads from the mesh and the input triangle mesh of the surface. Then we normalize this value by the average length of the horizontal and vertical foliation leaves containing this quad. Moreover, the area distortion stands for the difference between each quad and the corresponding area on the input surface. It is calculated by projecting each quad onto the input surface along the normal direction and compute the area distortion ratio between the two corresponding regions. The smaller the number is, the higher the accuracy will be. Table 2 shows that the reconstructed woven surfaces can approximate the input surfaces precisely, in which the average distance error is less than 1%.

It is remarkable that higher mesh resolution brings lower distance error and surface distortion. As shown in the first two rows in Table 2, comparing the human face model with quad mesh as 15 by 16 and 45 by 48, the average distance error reduces 86 %, and the average area distortion decreases from 6.49 % to 2.71 %. The size of cells in the weaving structure can also be adjusted. In particular, we can narrow the widths of strips in high curvature regions of the surface to improve the approximation accuracy (as shown in Fig. 18). Moreover, as this method guarantees that different leaves never intersect at non-singular points, the resolution of the weaving structure can be arbitrarily high to recover the input surface precisely.

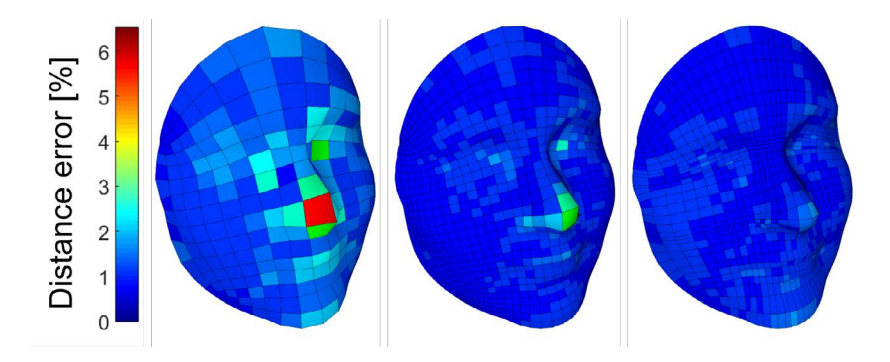


Figure 18: Surface distance error. Left to right: low resolution weaving structure, high resolution weaving structure and same high resolution weaving structure with modified grid distribution according to surface curvature distribution.

#### 6. Discussion and Conclusion

In summary, we utilize the mathematics theories of foliation in the engineering application of woven fabric, link the free-form spatial surface with the conventional in-plane textiles, and bring the conceptual digital woven surface design to practical fabrication of conformal thin shell structures.

The method is computationally efficient since the numerical generation of woven fabric is automatic. The foliation theory mathematically guarantees the robustness of the framework in three aspects. Firstly, the frame is not limited to certain types of surface topologies. Secondly, the woven fabric has a global tensor product structure with minimal singularities, and each leaf is smooth. According to Guass-Bonnet theorem, the total valence of singularities satisfies the condition  $\sum (4-k)\pi/2 = (2-2g)\pi 2$ . Suppose surface genus g is greater than zero. Because our method avoids valence 3 singularities, the number of singularities is less than that of conventional methods. In general, the number of singularities on a holomorphic one form is 2g-2, which on a holomorphic quadratic differential is 4g-4. Therefore the basic algorithm

produces the minimal number of singularities, though modifications may be made which introduce more singularities for the sake of better geometric fidelity. Moreover, the engineering requirements are satisfied: there is no T-junctions in the woven fabric; the crossing angles of every pair of threads are 90 degrees at non-singular regions.

In the current work, we focus on conformal woven fabrics at the macroscale and demonstrate our idea by weaving several models using construction paper. In the future, one can extend the work to weave a curved surface with a variety of material at different length scales, such as a car lining made by woven composite, a woven wearable electronics conformal to the human body, and woven surface meta-material design. Moreover, the proposed conformal weaving method gives a potential supplement to additive manufacturing. Combining with our proposed topology optimization framework-the extended level set method [68, 69, 70], we can offer a systematic solution from designing and fabricating structures on a surface with desired properties and performance.

However, there are some potential obstacles to the current method. First, the computation of the woven cells is automatic. Thus, the area of the woven cells may vary throughout the whole surface; the location of the singularities are automatically determined. In future research, we will work on improving the foliation computing method to produce consistent cells and offering user-input functionalities to better control the aesthetical and structural properties of the woven surface. Second, in the current work, the thickness of the surface is neglected, and the method performs well for fabricating thin shell structures. However, in real engineering applications, especially in ar-

chitecture, the thickness of the material is non-neglectable. While weaving, the bending of the thick stripes will induce extra rigidity and gaps between warps and wefts. Thus, in the future, we will improve the algorithm to balance the thickness effects. Furthermore, the fabrication is done manually, which is the most time-consuming step of the whole pipeline. In the future, we will consider cooperating with robotics in the weaving process.

## Acknowledgements

The project is partially supported by the National Natural Science Foundation of China (61720106005, 61772105, 61936002), NSF CMMI-1762287 collaborative research: computational framework for designing conformal stretchable electronics, Ford URP topology optimization of cellular mesostructures' nonlinear behaviors for crash safety, and NSF DMS-1737812 collaborative research: ATD: theory and algorithms for discrete curvatures on network data from human mobility and monitoring.

## References

- [1] T. D. Ngo, A. Kashani, G. Imbalzano, K. T. Nguyen, D. Hui, Additive manufacturing (3D printing): A review of materials, methods, applications and challenges, Composites Part B: Engineering 143 (2018) 172–196.
- [2] S. Waheed, J. M. Cabot, N. P. Macdonald, T. Lewis, R. M. Guijt, B. Paull, M. C. Breadmore, 3D printed microfluidic devices: enablers and barriers, Lab on a Chip 16 (11) (2016) 1993–2013.

- [3] B. K. Behera, P. Hari, Woven textile structure: Theory and applications, Elsevier, 2010.
- [4] P. Boisse, Composite reinforcements for optimum performance, Elsevier, 2011.
- [5] Y. Zhang, S. Ha, K. Sharp, J. K. Guest, T. Weihs, K. J. Hemker, Fabrication and mechanical characterization of 3D woven Cu lattice materials, Materials & Design 85 (2015) 743–751.
- [6] S. M. Ryan, S. Szyniszewski, S. Ha, R. Xiao, T. D. Nguyen, K. W. Sharp, T. P. Weihs, J. K. Guest, K. J. Hemker, Damping behavior of 3D woven metallic lattice materials, Scripta Materialia 106 (2015) 1–4.
- [7] R. Wu, L. Ma, C. Hou, Z. Meng, W. Guo, W. Yu, R. Yu, F. Hu, X. Y. Liu, Silk composite electronic textile sensor for high space precision 2D combo temperature–pressure sensing, Small (2019) 1901558.
- [8] T. Zhou, C. Zhang, C. B. Han, F. R. Fan, W. Tang, Z. L. Wang, Woven structured triboelectric nanogenerator for wearable devices, ACS applied materials & interfaces 6 (16) (2014) 14695–14701.
- [9] Airbus, The A350-900 visits MAKS air show in Russia, https://www.airbus.com/newsroom/press-releases/en/2017/07/ the-a350-900-visits-maks-air-show-in-russia.html (2017).
- [10] X. Pu, L. Li, M. Liu, C. Jiang, C. Du, Z. Zhao, W. Hu, Z. L. Wang, Wearable self-charging power textile based on flexible yarn supercapacitors and fabric nanogenerators, Advanced Materials 28 (1) (2016) 98–105.

- [11] A. Drach, B. Drach, I. Tsukrov, Processing of fiber architecture data for finite element modeling of 3D woven composites, Advances in Engineering Software 72 (2014) 18–27.
- [12] A. Miravete, 3-D textile reinforcements in composite materials, Woodhead Publishing, 1999.
- [13] D. Coupé, Woven reinforcements for composites, in: Composite reinforcements for optimum performance, Elsevier, 2011, pp. 89–115.
- [14] N. Khokar, 3D-weaving: theory and practice, Journal of the Textile Institute 92 (2) (2001) 193–207.
- [15] B. Behera, R. Mishra, 3-Dimensional weaving, Indian Journal of Fibre Textile Research 33 (3) (2008) 274–287.
- [16] M. Mohamed, A. Bogdanovich, Comparative analysis of different 3D weaving processes, machines and products, in: Proceedings of the 17th International Conference on Composite Materials (ICCM-17), 2009, pp. 27–31.
- [17] H. M. El-Dessouky, M. N. Saleh, 3D woven composites: from weaving to manufacturing, Recent Developments in the Field of Carbon Fibers (2018) 51.
- [18] L. Zhao, S. M. Ryan, J. K. Ortega, S. Ha, K. W. Sharp, J. K. Guest, K. J. Hemker, T. P. Weihs, Experimental investigation of 3D woven Cu lattices for heat exchanger applications, International Journal of Heat and Mass Transfer 96 (2016) 296–311.

- [19] X. Wang, B. Hu, Y. Feng, F. Liang, J. Mo, J. Xiong, Y. Qiu, Low velocity impact properties of 3D woven basalt/aramid hybrid composites, Composites Science and Technology 68 (2) (2008) 444–450.
- [20] W.-S. Kuo, T.-H. Ko, C.-P. Chen, Effect of weaving processes on compressive behavior of 3D woven composites, Composites Part A: Applied Science and Manufacturing 38 (2) (2007) 555–565.
- [21] M. Bannister, R. Braemar, P. Crothers, The mechanical performance of 3D woven sandwich composites, Composite Structures 47 (1-4) (1999) 687–690.
- [22] M. Stoppa, A. Chiolerio, Wearable electronics and smart textiles: a critical review, sensors 14 (7) (2014) 11957–11992.
- [23] W. Zeng, L. Shu, Q. Li, S. Chen, F. Wang, X.-M. Tao, Fiber-based wearable electronics: a review of materials, fabrication, devices, and applications, Advanced materials 26 (31) (2014) 5310–5336.
- [24] M. A. Case, H. A. Burwick, K. G. Volpp, M. S. Patel, Accuracy of smartphone applications and wearable devices for tracking physical activity data, Jama 313 (6) (2015) 625–626.
- [25] Y. Liu, M. Pharr, G. A. Salvatore, Lab-on-skin: a review of flexible and stretchable electronics for wearable health monitoring, ACS nano 11 (10) (2017) 9614–9635.
- [26] H.-Y. Jeon, Woven fabrics, BoD–Books on Demand, 2012.

- [27] X. Chen, A. Ebru Tayyar, Engineering, manufacturing, and measuring 3D domed woven fabrics, Textile research journal 73 (5) (2003) 375–380.
- [28] R. Manjunath, B. K. Behera, Emerging trends in 3D woven preforms for composite reinforcements, Advanced Textile Engineering Materials (2018) 463–497.
- [29] S. Sharma, M. Sutcliffe, Draping of woven composites over irregular surfaces, in: Proceedings of the 13th International Conference on Composite Materials (ICCM-13), Beijing, China, 2001.
- [30] K. Buet-Gautier, P. Boisse, Experimental analysis and modeling of biaxial mechanical behavior of woven composite reinforcements, Experimental mechanics 41 (3) (2001) 260–269.
- [31] P. G. Unal, 3D woven fabrics, woven fabrics, Han-Yong Jean (Ed.), ISBN: 978-953-51-0607-4, InTech (2012).
- [32] G. Hivet, P. Boisse, Consistent mesoscopic mechanical behaviour model for woven composite reinforcements in biaxial tension, Composites Part B: Engineering 39 (2) (2008) 345–361.
- [33] J. Xue, K. Kirane, Strength size effect and post-peak softening in textile composites analyzed by cohesive zone and crack band models, Engineering Fracture Mechanics 212 (2019) 106–122.
- [34] G. Max, The weaving pavilion at Notch 10 Art Culture Festival, Beijing, http://davidgarciastudio.blogspot.com/2009/04/weaving-project.html (2010).

- [35] F. Giuseppe, S. Stefan, Woven tower mimics local palm-weaving techniques, http://www.evolo.us/woven-tower-mimics-local-palm-weaving-techniques/ (2012).
- [36] M. Georgiou, O. Georgiou, C. Williams, Iterating Towards Affordability, in: Modelling Behaviour, Springer, 2015, pp. 517–526.
- [37] T. Simmonds, M. Self, D. Bosia, Woven surface and form, Architectural Design 76 (6) (2006) 82–89.
- [38] B. Quinn, Textiles in architecture, Architectural Design 76 (6) (2006) 22–26.
- [39] M. R. Thomsen, K. Bech, K. Sigurdardottir, Textile logics in a digital architecture, New Design Concepts and Strategies 2 (2012) 611–618.
- [40] E. Akleman, J. Chen, Q. Xing, J. L. Gross, Cyclic plain-weaving on polygonal mesh surfaces with graph rotation systems 28 (3) (2009) 78.
- [41] E. Akleman, J. Chen, Y. Chen, Q. Xing, J. L. Gross, Cyclic twill-woven objects, Computers & Graphics 35 (3) (2011) 623–631.
- [42] Q. Xing, G. Esquivel, R. Collier, M. Tomaso, E. Akleman, et al., Spulenkorb: utilize weaving methods in architectural design, 2011, pp. 164–170.
- [43] M. Campen, D. Bommes, L. Kobbelt, Dual loops meshing: quality quad layouts on manifolds, ACM Transactions on Graphics (TOG) 31 (4) (2012) 110.

- [44] S. D. Pandita, K. Nishiyabu, I. Verpoest, Strain concentrations in woven fabric composites with holes, Composite Structures 59 (3) (2003) 361– 368.
- [45] A. Yudhanto, Mechanical characteristics and damage mechanisms of stitched carbon/epoxy composites under static and fatigue loads, Ph.D. thesis, Tokyo Metropolitan University (2013).
- [46] J. Vekhter, J. Zhuo, L. F. G. Fandino, Q. Huang, E. Vouga, Weaving geodesic foliations, ACM Transactions on Graphics (TOG) 38 (4) (2019) 34.
- [47] P. Ayres, A. G. Martin, M. Zwierzycki, Beyond the Basket Case: a principled approach to the modelling of Kagome weave patterns for the fabrication of interlaced lattice structures using straight strips, in: Advances in Architectural Geometry 2018, Chalmers University of Technology, 2018, pp. 72–93.
- [48] M. Takezawa, T. Imai, K. Shida, T. Maekawa, Fabrication of freeform objects by principal strips, ACM Transactions on Graphics (TOG) 35 (6) (2016) 225.
- [49] M. Campen, L. Kobbelt, Dual strip weaving: interactive design of quad layouts using elastica strips, ACM Transactions on Graphics (TOG) 33 (6) (2014) 183.
- [50] N. Lei, X. Zheng, Z. Luo, F. Luo, X. Gu, Quadrilateral Mesh Generation II: Meromorphic Quartic Differentials and Abel-Jacobi Condition, arXiv preprint cs/1907.00216.

- [51] W. P. Thurston, et al., On the geometry and dynamics of diffeomorphisms of surfaces, Bulletin (new series) of the american mathematical society 19 (2) (1988) 417–431.
- [52] J. Hubbard, H. Masur, Quadratic differentials and foliations, Acta Mathematica 142 (1) (1979) 221–274.
- [53] K. Strebel, Über quadratische Differentiale mit geschlossenen Trajektorien und extremale quasikonforme Abbildungen, in: Festband zum 70. Geburtstag von Rolf Nevanlinna, Springer, 1966, pp. 105–127.
- [54] X. Gu, S.-T. Yau, Global conformal surface parameterization, in: Proceedings of the 2003 Eurographics/ACM SIGGRAPH symposium on Geometry processing, Eurographics Association, 2003, pp. 127–137.
- [55] N. Lei, X. Zheng, H. Si, Z. Luo, X. Gu, Generalized Regular Quadrilateral Mesh Generation based on Surface Foliation, Procedia engineering 203 (2017) 336–348.
- [56] N. Lei, X. Zheng, J. Jiang, Y.-Y. Lin, D. X. Gu, Quadrilateral and hexahedral mesh generation based on surface foliation theory, Computer Methods in Applied Mechanics and Engineering 316 (2017) 758–781.
- [57] N. Lei, X. Zheng, Z. Luo, D. X. Gu, Quadrilateral and hexahedral mesh generation based on surface foliation theory II, Computer Methods in Applied Mechanics and Engineering 321 (2017) 406–426.
- [58] A. Hatcher, Pants Decompositions of Surfaces (1999). arXiv:math/9906084.

- [59] X. Li, X. Gu, H. Qin, Surface mapping using consistent pants decomposition, IEEE Trans. Vis. Comput. Graph. 15 (4) (2009) 558–571.
- [60] T. Dey, K. Li, J. Sun, On computing handle and tunnel loops, in: International Conf. on Cyberworlds, 2007, pp. 357–366.
- [61] K. Strebel, Quadratic Differentials, Ergebnisse der Mathematik und ihrer Grenzgebiete. 3. Folge A Series of Modern Surveys in Mathematics, Springer, 1984.
  - URL https://books.google.com/books?id=hiI96XVWdb0C
- [62] M. Wolf, On realizing measured foliations via quadratic differentials of Harmonic maps to R-trees, J. D'Analyse Math (1996) 107–120.
- [63] R. M. Schoen, S.-T. Yau, Lectures on harmonic maps, Vol. 2, Amer Mathematical Society, 1997.
- [64] X. Gu, T.-T. Yau, Computational Conformal Geometry, International Press of Boston, Inc., 2008.
- [65] H. Pottmann, A. Schifter, P. Bo, H. Schmiedhofer, W. Wang, N. Bal-dassini, J. Wallner, Freeform Surfaces from Single Curved Panels, in: Proceedings of ACM SIGGRAPH 2008, 2008, pp. 1–10.
- [66] A. Allaoui, S. Bai, H.-M. Cheng, J. Bai, Mechanical and electrical properties of a MWNT/epoxy composite, Composites science and technology 62 (15) (2002) 1993–1998.
- [67] C. Knauer, Algorithms for comparing geometric patterns, Ph.D. thesis, Citeseer (2001).

- [68] Q. Ye, Y. Guo, S. Chen, X. D. Gu, N. Lei, Topology optimization of conformal structures using extended level set methods and conformal geometry theory, in: ASME 2018 International Design Engineering Technical Conferences and Computers and Information in Engineering Conference, American Society of Mechanical Engineers Digital Collection.
- [69] Q. Ye, Y. Guo, S. Chen, N. Lei, X. D. Gu, Topology optimization of conformal structures on manifolds using extended level set methods (X-LSM) and conformal geometry theory, Computer Methods in Applied Mechanics and Engineering 344 (2019) 164–185.
- [70] Q. Ye, L. Jiang, S. Chen, X. D. Gu, Generative design of multi-functional conformal structures using extended level set methods (X-LSM) and conformal geometry theory (pre-print).